

# DYNAMIC RESPONSE ANALYSIS OF SUBMERGED SOIL BY THIN LAYERED ELEMENT METHOD

by

Toyoaki Nogami<sup>1</sup> and Motoki Kazama<sup>2</sup>

**ABSTRACT:** A thin layered element method is formulated to compute the dynamic response of submerged soil. The formulation is based on Biot's equation describing the dynamic behavior of fluid-saturated elasto-porous medium. The dynamic response of submerged soil is computed for various cases by using the developed formulation. The effects of submerged conditions are examined for submerged soil deposits with a water level at and above the ground surface. It is found that both submerged conditions and water above the ground surface can considerably affect the dynamic response of soil deposits.

## INTRODUCTION

When the dynamic load is applied to saturated soil, pore fluid movement relative to soil skeleton may be induced. The transient movement and redistribution of pore fluid can significantly affect the dynamic response soil behavior. Those are generally governed by the loading rate, soil permeability, pressure gradient and boundary conditions, resulting in an extremely complex picture of the dynamic response behavior of submerged soil.

Biot (1962) has made a framework in the formulation of dynamic response of fluid-filled elasto-porous medium. This formulation has been generally used for dynamic response analysis of submerged soil and evaluated typically by either analytical solutions obtained by solving the differential equations or the numerical finite element method. Considerable difficulty exists in obtaining analytical solutions for Biot's equation in general and thus the solutions have been developed only for very simple conditions (e.g. Biot, 1956; Jones, 1961; Deresiewics, 1960; Foda and Mei, 1982). Those conditions are generally far from those commonly encountered in the real situation. The finite element

1. Associate Head of Ocean Engineering, Scripps Inst. of Oceanography, Univ. of Calif., La Jolla, CA 92093
2. Senior Research Engineer, Port and Harbor Research Institute, Ministry of Transport, Kurihama, Kanagawa, Japan.

method has been applied for the numerical evaluation of Biot's equation (e.g. Ghaboussi and Wilson, 1973; Prevost, 1982; Simon et al., 1986; Zienkiewicz et al., 1977). Contrary to the former approach, this approach can account for complex geometry and inhomogeneity without increasing the degree of difficulty and amount of computation. However, compared with the finite element scheme applied to a single-phase medium, the computation effort increases substantially due to the additional degrees of freedom associated with pore fluid. A thin layered element method has been developed by combining the finite element method and analytical solution, to compute the responses by using Rayleigh wave modes (Kausel and Roesset, 1975; Lysmer and Waas, 1972; Tajimi and Shimomura, 1976). This approach requires computation effort far less than the regular finite element approach and yet has a capacity of accommodating complex conditions far more than the approach with analytical solution. It has been applied to the dynamic response computation of a single-phase medium but not yet to a fluid-saturated porous medium. For the dynamic response analysis of a two-phase mixture, this approach appears to be very attractive because a large computation effort is generally required in such analysis by the regular finite element method.

## FORMULATION

The soil medium is assumed to be an elastic porous medium saturated with pore fluid. The displacement of the pore fluid relative to the displacement of the solid skeleton is defined as

$$\mathbf{w} = n(\mathbf{U} - \mathbf{u}) \quad (1)$$

where  $n$  = porosity;  $\mathbf{w} = (w_x, w_z)^T$  in which  $w_j$  is relative displacement of fluid in the  $j$  direction;  $\mathbf{u} = (u_x, u_z)^T$  in which  $u_j$  is displacements of solid skeleton in the  $j$  direction;  $\mathbf{U} = (U_x, U_z)^T$  in which  $U_j$  is the average displacement of the fluid in the  $j$  direction so as to be a

volume of fluid displaced through a unit area of the mixture perpendicular to the displacement; and  $x$  and  $z$  = Cartesian coordinates in horizontal and vertical directions, respectively. The total normal stresses acting on a unit area of mixture is

$$\sigma = (1-n)\sigma_s - mn\pi = \sigma' - mn\pi \quad (2)$$

where  $\sigma_s = (\sigma_{sx}, \sigma_{sz}, \tau_{xz})^T$  in which  $\sigma_{sj}$  is a normal stress in the  $j$  direction acting on the solid skeleton averaged over the unit area;  $\sigma = (\sigma_x, \sigma_y, \tau_{xz})^T$  in which  $\sigma_j$  is a total normal stress in the  $j$  direction;  $\sigma' = (\sigma'_x, \sigma'_z, \tau_{xz})^T$  in which  $\sigma'_j$  is an effective normal stress in the  $j$  direction;  $\tau_{xz}$  = shear stress;  $\pi$  = pore fluid pressure; and  $\mathbf{m} = (1,1,0)^T$ .

The equilibrium condition of forces acting on the soil skeleton in a unit soil volume is described as

$$(1-n)\mathbf{L}^T\sigma_s + (1-n)\rho_s\mathbf{b} + nk^{-1}\dot{\mathbf{w}} = (1-n)\rho_s\ddot{\mathbf{u}} \quad (3)$$

where  $\mathbf{w} = \partial\mathbf{w}/\partial t$ ;  $\mathbf{u} = \partial^2\mathbf{u}/\partial t^2$ ;  $\mathbf{b} = (b_x, b_z)^T$  in which  $b_j$  is body force in the  $j$  direction per unit mass;  $\rho_s$  = density of a unit volume of the solid material in the skeleton; and

$$\mathbf{L}^T = \begin{bmatrix} \frac{\partial}{\partial x} & 0 & \frac{\partial}{\partial z} \\ 0 & \frac{\partial}{\partial z} & \frac{\partial}{\partial x} \end{bmatrix} \quad (4)$$

The equilibrium condition of the forces acting on the pore fluid domain in a unit volume of soil is given by

$$n\nabla\pi - k^{-1}n\dot{\mathbf{w}} + n\rho_f\mathbf{b} = \rho_f\dot{\mathbf{w}} + n\rho_f\ddot{\mathbf{u}} \quad (5)$$

where  $\rho_f$  = density of unit volume of pore fluid; and  $\nabla = (\partial/\partial x, \partial/\partial z)^T$ . Combining Eqs. 3 and 5, the equilibrium condition of the pore fluid and solid skeleton mixture is expressed as

$$\mathbf{L}^T \boldsymbol{\sigma} + \rho \mathbf{b} = \rho \ddot{\mathbf{u}} + \rho_f \dot{\mathbf{w}} \quad (6)$$

where  $\rho$  = density of unit volume of mixture =  $(1-n)\rho_s + n\rho_f$ . Since linear elastic conditions are considered, body forces will be neglected hereafter.

The rate of the fluid stored in a unit volume mixture is equal to the summation of the rate of the volume change of volumetric strain in the solid, the rate of change due to compression of the solid by pore fluid pressure, the rate of change due to compression of the solid by the effective stresses, and the rate of change due to compressibility of the fluid. According to Simon et al. (1984), this is expressed as

$$\nabla^T \mathbf{w} = -\alpha \mathbf{m}^T \boldsymbol{\varepsilon} + Q^{-1} \pi \quad (7)$$

where  $\boldsymbol{\varepsilon}$  = strains =  $(\varepsilon_x, \varepsilon_z, \gamma_{xz})^T$ ; and  $\alpha$  and  $Q$  are related with material properties through

$$\alpha = 1 - \frac{K_d}{K_s} \quad \text{and} \quad Q^{-1} = \frac{1}{K_f} + \frac{\alpha-n}{K_s} \quad (8)$$

where  $K_s$  = elastic volumetric modulus of solid;  $K_f$  = volumetric modulus of fluid; and  $K_d$  = elastic volumetric modulus of solid skeleton. Substituting  $\pi$  in Eq. 7 into Eq. 2 and using the stress-strain relationship,  $\boldsymbol{\sigma}' = \mathbf{D}\boldsymbol{\varepsilon}$ , the total stresses,  $\boldsymbol{\sigma}$ , can be correlated with  $\boldsymbol{\varepsilon}$  and  $\mathbf{w}$ . With  $\boldsymbol{\varepsilon} = \mathbf{L}\mathbf{u}$ , this expression and pore fluid pressure given in Eq. 7 can be written in a matrix form such that

$$\begin{Bmatrix} \boldsymbol{\sigma} \\ \pi \end{Bmatrix} = \begin{bmatrix} (\mathbf{D} + \alpha^2 \mathbf{Q} \mathbf{m} \mathbf{m}^T) \mathbf{L} & \alpha \mathbf{Q} \mathbf{m} \nabla^T \\ \alpha \mathbf{Q} \mathbf{m}^T & \mathbf{Q} \nabla^T \end{bmatrix} \begin{Bmatrix} \mathbf{u} \\ \mathbf{w} \end{Bmatrix} \quad (9)$$

Using  $\pi$  and  $\boldsymbol{\sigma}$  defined in Eq. 9, Eqs. 5 and 6 can be rewritten in the following matrix form after using the relationship  $\boldsymbol{\varepsilon} = \mathbf{L}\mathbf{u}$  :

$$\mathbf{M} \begin{Bmatrix} \ddot{\mathbf{u}} \\ \ddot{\mathbf{w}} \end{Bmatrix} + \mathbf{C} \begin{Bmatrix} \dot{\mathbf{u}} \\ \dot{\mathbf{w}} \end{Bmatrix} + \mathbf{K} \begin{Bmatrix} \mathbf{u} \\ \mathbf{w} \end{Bmatrix} = \begin{Bmatrix} \mathbf{0} \\ \mathbf{0} \end{Bmatrix} \quad (10)$$

where

$$\mathbf{M} = \begin{bmatrix} \rho & \rho_f \\ \rho_f & \rho_f/n \end{bmatrix} \quad \mathbf{C} = \begin{bmatrix} 0 & 0 \\ 0 & k^{-1} \end{bmatrix} \quad \mathbf{K} = \begin{bmatrix} \mathbf{L}^T (\mathbf{D} + \alpha^2 \mathbf{Q} \mathbf{m} \mathbf{m}^T) \mathbf{L} & \alpha \mathbf{Q} \mathbf{L}^T \mathbf{m} \mathbf{V}^T \\ \alpha \mathbf{Q} \mathbf{V} \mathbf{m}^T \mathbf{L} & \mathbf{Q} \mathbf{V} \mathbf{V}^T \end{bmatrix} \quad (11)$$

Consider horizontally layered submerged soil. The displacements of the medium in the wave field is expressed in the form of  $(\mathbf{u}(x,z,t), \mathbf{w}(x,z,t)) = (\mathbf{u}(x), \mathbf{w}(z))e^{-i(\omega t - hx)}$  in which  $\omega$  = circular frequency and  $h$  = wave number. Using a shape function in  $z$  direction and omitting the time factor, the displacements of the  $j$ th layer in the wave field are approximately expressed by using the displacements at the upper and lower ends of the  $j$ th layer as

$$\begin{Bmatrix} \mathbf{u}_j(x,z) \\ \mathbf{w}_j(x,z) \end{Bmatrix} = e^{-ihx} \mathbf{Z}(z) \begin{Bmatrix} \mathbf{U}_j \\ \mathbf{W}_j \end{Bmatrix} \quad (12)$$

where  $e^{-ihx} \mathbf{U}_j^T = (\mathbf{u}_j(x,0))^T, \mathbf{u}_j(x,H_j)^T$  and  $e^{-ihx} \mathbf{W}_j^T = (\mathbf{w}_j(x,0))^T, \mathbf{w}_j(x,H_j)^T$ , in which  $z=0$  and  $H_j$  indicate respectively the upper end and lower ends of the  $j$ th layer; ; and  $\mathbf{Z}(z)$  = matrix containing shape function . When linear variations of the displacements are assumed along  $z$ , the shape function matrix  $\mathbf{Z}$  is

$$\mathbf{Z}(z) = \begin{pmatrix} 1 - \frac{z}{H_j} & \frac{z}{H_j} \end{pmatrix} \mathbf{I} \quad (13)$$

where  $\mathbf{I} = 4 \times 4$  identity matrix. It is noted in Eq. 13 that the factor  $(1-z/H_j, z/H_j)$  is simply multiplied to the numbers in  $\mathbf{I}$  and thus  $\mathbf{Z}$  is a matrix with 4 rows and 8 columns. The time factor,  $e^{i\omega t}$ , will be omitted hereafter.

After substituting Eq. 12 into Eq. 10, Galarkin's procedure applied to Eq. 10 results in

$$\sum_{j=1}^J \int_0^{H_j} \mathbf{Z}^T \left( \mathbf{K}_j + i\omega \mathbf{C}_j - \omega^2 \mathbf{M}_j \right) \mathbf{Z} \begin{Bmatrix} \mathbf{U}_j \\ \mathbf{W}_j \end{Bmatrix} e^{-ihx} dz - \sum_{j=1}^J \mathbf{Z}^T \left( \mathbf{K}'_j + i\omega \mathbf{C}'_j - \omega^2 \mathbf{M}'_j \right) \mathbf{Z} \begin{Bmatrix} \mathbf{U}_j \\ \mathbf{W}_j \end{Bmatrix} e^{-ihx} \Big|_0^{H_j} = \mathbf{0} \quad (14)$$

where  $J$  = numbers of layers; and  $(\mathbf{K}', \mathbf{C}', \mathbf{M}') = \int (\mathbf{K}, \mathbf{C}, \mathbf{M}) dz$ . The inside of the second summation in Eq. 14,  $S$ , can be rewritten as

$$\begin{aligned} S &= \int_0^{H_j} \frac{\partial}{\partial z} \left\{ \mathbf{Z}^T \left( \mathbf{K}'_j + i\omega \mathbf{C}'_j - \omega^2 \mathbf{M}'_j \right) \mathbf{Z} \begin{Bmatrix} \mathbf{U}_j \\ \mathbf{W}_j \end{Bmatrix} e^{-ihx} \right\} dz \\ &= \int_0^{H_j} \frac{\partial \mathbf{Z}^T}{\partial z} \left( \mathbf{K}'_j + i\omega \mathbf{C}'_j - \omega^2 \mathbf{M}'_j \right) \mathbf{Z} \begin{Bmatrix} \mathbf{U}_j \\ \mathbf{W}_j \end{Bmatrix} e^{-ihx} dx + \int_0^{H_j} \mathbf{Z} \frac{\partial}{\partial z} \left( \mathbf{K}'_j + i\omega \mathbf{C}'_j - \omega^2 \mathbf{M}'_j \right) \mathbf{Z} \begin{Bmatrix} \mathbf{U}_j \\ \mathbf{W}_j \end{Bmatrix} dz \end{aligned} \quad (15)$$

Substituting Eq. 15 into Eq. 14 and performing integration with respect to  $z$  result in the characteristics equation in the discretized form such that

$$\sum_{j=1}^J \left( h^2 \alpha_j + ih\beta_j + \gamma_j \right) \begin{Bmatrix} \mathbf{U}_j \\ \mathbf{W}_j \end{Bmatrix} = \mathbf{0}$$

or

$$\left( h^2 \alpha + ih\beta + \gamma \right) \begin{Bmatrix} \mathbf{U} \\ \mathbf{W} \end{Bmatrix} = \mathbf{0} \quad (16)$$

where

$$\begin{aligned}
\alpha_j &= \frac{H_j}{6} \begin{bmatrix} Aa & 0a & \alpha Qa & 0a \\ 0a & Ga & 0a & 0a \\ \alpha Qa & Qa & Qa & 0a \\ 0a & 0a & 0a & 0a \end{bmatrix} \\
\beta_j &= \frac{1}{2} \begin{bmatrix} 0b (A-2G)b & 0b & \alpha Qb \\ Gb & 0b & 0b & 0b \\ 0b & \alpha Qb & 0b & Qb \\ 0b & 0b & 0b & 0b \end{bmatrix}^T - \frac{1}{2} \begin{bmatrix} 0b (A-2G)b & 0b & \alpha Qb \\ Gb & 0b & 0b & 0b \\ 0b & \alpha Qb & 0b & Qb \\ 0b & 0b & 0b & 0b \end{bmatrix} \\
\gamma_j &= \frac{1}{H_j} \begin{bmatrix} Gc & 0c & 0c & 0c \\ 0c & Ac & 0c & \alpha Qc \\ 0c & 0c & 0c & 0c \\ 0c & \alpha Qc & 0c & Qc \end{bmatrix} + i\omega \frac{H_j}{6} \begin{bmatrix} 0a & 0a & 0a & 0a \\ 0a & 0a & 0a & 0a \\ 0a & 0a & k^{-1}a & 0a \\ 0a & 0a & 0a & k^{-1}a \end{bmatrix} - \\
&\quad \omega^2 \frac{H_j}{6} \begin{bmatrix} \rho a & 0a & \rho_f a & 0a \\ 0a & \rho a & 0a & \rho_f a \\ \rho_f a & 0a & \rho_f / na & 0a \\ 0a & \rho_f a & 0a & \rho_f / na \end{bmatrix}
\end{aligned} \tag{17}$$

in which  $A = \lambda + 2G + \alpha^2 Q$ ; and

$$\mathbf{a} = \begin{bmatrix} 2 & 1 \\ 1 & 2 \end{bmatrix} \quad \mathbf{b} = \begin{bmatrix} 1 & -1 \\ 1 & -1 \end{bmatrix} \quad \mathbf{c} = \begin{bmatrix} 1 & -1 \\ -1 & 1 \end{bmatrix} \tag{18}$$

Wave numbers,  $h$ , and their associated mode shape vectors,  $(\phi_u^T, \phi_w^T)^T$ , can be determined by solving the characteristic equation Eq. 16. Since the fluid pressure is an all round equal pressure, there is a constraintment between the freedoms associated with  $w_x$  and  $w_z$  and therefore the characteristic equation for  $J$  layers results in the number of eigenvalues equal to  $3J$  conjugate pairs instead of  $4J$ . In order to satisfy the wave scattering conditions, only those with the plus sign in the imaginary part are selected among the conjugate pairs. Then, the displacements of the submerged layered-soil is expressed along  $x$  at the nodal points as

$$\begin{Bmatrix} \mathbf{U}(x) \\ \mathbf{W}(x) \end{Bmatrix} = \sum_{s=1}^{3J} e^{-ih_s x} \alpha_s \begin{Bmatrix} \phi_u \\ \phi_w \end{Bmatrix}_s$$

and thus the displacements within the  $j$ th layer as

$$\begin{Bmatrix} \mathbf{u}_j(x,z) \\ \mathbf{w}_j(x,z) \end{Bmatrix} = \mathbf{Z}(z) \sum_{s=1}^{3J} e^{-ih_s x} \alpha_s \begin{Bmatrix} \phi_{uj} \\ \phi_{wj} \end{Bmatrix}_s \quad (19)$$

where  $(\phi_{\mathbf{u}}^T, \phi_{\mathbf{w}}^T)_s^T =$  sth eigenvector in which  $\phi_{\mathbf{u}}$  and  $\phi_{\mathbf{w}} =$  vectors of size  $2J$ ;  $\phi_{uj}$  and  $\phi_{wj} =$  vectors containing the values at the locations corresponding the  $j$ th layer in  $\phi_{\mathbf{u}}$  and  $\phi_{\mathbf{w}}$ , respectively;  $h_s =$  sth eigenvalue; and  $\alpha_s =$  sth mode participation factor. Then, using Eqs. 9 and 19 together with Eq. 13, the stresses and pore fluid pressure at the middle of the  $j$ th layer are

$$\begin{Bmatrix} \sigma_j(x, 0.5H_j) \\ \pi_j(x, 0.5H_j) \end{Bmatrix} = -i A_j \sum_{s=1}^{3J} h_s e^{-ih_s x} \alpha_s \begin{Bmatrix} \phi_{uj} \\ \phi_{wj} \end{Bmatrix}_s + \mathbf{B}_j \sum_{s=1}^{3J} e^{-ih_s x} \alpha_s \begin{Bmatrix} \phi_{uj} \\ \phi_{wj} \end{Bmatrix}_s \quad (20)$$

where

$$\mathbf{A}_j = \frac{1}{2} \begin{bmatrix} A & A & 0 & 0 & \alpha Q & \alpha Q & 0 & 0 \\ A-2G & A-2G & 0 & 0 & \alpha Q & \alpha Q & 0 & 0 \\ 0 & 0 & G & G & 0 & 0 & 0 & 0 \\ \alpha Q & \alpha Q & 0 & 0 & Q & Q & 0 & 0 \end{bmatrix} \quad (21)$$

$$\mathbf{B}_j = \frac{1}{H_j} \begin{bmatrix} 0 & 0 & -(A-2G) & (A-2G) & 0 & 0 & -\alpha Q & \alpha Q \\ 0 & 0 & -A & A & 0 & 0 & -\alpha Q & \alpha Q \\ -G & G & 0 & 0 & 0 & 0 & 0 & 0 \\ 0 & 0 & -\alpha Q & \alpha Q & 0 & 0 & -Q & Q \end{bmatrix}$$

A vertical cut is considered at  $x=0$  in a layered soil. After substituting Eqs. 13 and 19 into Eq. 9, the nodal forces acting on the vertical cut of the  $j$ th layer for  $x \geq 0$  can be obtained as

$$\begin{Bmatrix} \mathbf{P}_{xj} \\ \mathbf{P}_{zj} \\ \mathbf{P}_{\pi j} \end{Bmatrix} = i \mathbf{E}_j \sum_{s=1}^{3J} h_s \alpha_s \begin{Bmatrix} \phi_{uj} \\ \phi_{wxj} \end{Bmatrix}_s + \mathbf{F}_j \sum_{s=1}^{3J} \alpha_s \begin{Bmatrix} \phi_{uj} \\ \phi_{wzj} \end{Bmatrix}_s \quad (22)$$

where

$$\begin{Bmatrix} \mathbf{P}_{xj} \\ \mathbf{P}_{zj} \\ \mathbf{P}_{\pi j} \end{Bmatrix} = - \int_0^{H_j} \mathbf{N}^T \begin{Bmatrix} \alpha_{xj}(0,z) \\ \tau_{xzj}(0,z) \\ \pi_j(0,z) \end{Bmatrix} dz$$

$$\mathbf{E}_j = \frac{H_j}{6} \begin{bmatrix} Aa & 0a & \alpha Qa \\ 0a & Ga & 0a \\ \alpha Qa & 0a & Qa \end{bmatrix} \quad \text{with} \quad \mathbf{a} = \begin{bmatrix} 2 & 1 \\ 1 & 2 \end{bmatrix} \quad (23)$$

$$\mathbf{F}_j = \frac{1}{2} \begin{bmatrix} 0b & (A-2G)b & \alpha Qb \\ Gb & 0b & 0b \\ 0b & \alpha b & Qb \end{bmatrix} \quad \text{with} \quad \mathbf{b} = \begin{bmatrix} 1 & -1 \\ 1 & -1 \end{bmatrix}$$

Therefore those of the entire layered system for  $x \geq 0$  are

$$\begin{Bmatrix} \mathbf{P}_x \\ \mathbf{P}_z \\ \mathbf{P}_\pi \end{Bmatrix} = i \mathbf{E} \sum_{s=1}^{3J} h_s \alpha_s \begin{Bmatrix} \phi_u \\ \phi_{wx} \end{Bmatrix}_s + \mathbf{F} \sum_{s=1}^{3J} \alpha_s \begin{Bmatrix} \phi_u \\ \phi_{wz} \end{Bmatrix}_s$$

or

$$\begin{Bmatrix} \mathbf{P}_x \\ \mathbf{P}_z \\ \mathbf{P}_\pi \end{Bmatrix} = (i \mathbf{E} \phi' + \mathbf{F} \phi'') \alpha \quad (24)$$

where  $\phi'$  and  $\phi'' = 3J \times 3J$  matrices containing the vectors  $h_s(\phi_u^T, \phi_{wx}^T)_s^T$  and  $(\phi_u^T, \phi_{wz}^T)_s^T$  at the  $s$ th column, respectively; and  $\alpha =$  vector containing  $\alpha_s$  at the  $s$ th location. Given external loads at  $x=0$ ,  $(\mathbf{Q}_x, \mathbf{Q}_z, \mathbf{Q}_\pi)$ , the participation factors,  $\alpha$ , can be determined from Eq. 24 with  $(\mathbf{P}_x, \mathbf{P}_z, \mathbf{P}_\pi) = (\mathbf{Q}_x, \mathbf{Q}_z, \mathbf{Q}_\pi)/2$  and  $(\mathbf{P}_x, \mathbf{P}_z, \mathbf{P}_\pi) = (\mathbf{Q}_x, \mathbf{Q}_z, \mathbf{Q}_\pi)$  for the soil medium extending respectively through  $-\infty \leq x \leq +\infty$  and  $0 \leq x \leq +\infty$ .

With those participation factors, the displacements can be determined from Eq. 19 and the stresses and pore pressure from Eq. 20.

It is noted that , when the layer is made of fluid only, Eq. 10 and all other formulations can be rewritten with  $\mathbf{u} = \mathbf{0}$ ,  $k = \infty$ ,  $n = 1$  and  $Q = 1/K_f$ . The undrained condition corresponds to  $w = 0$  and  $k = 0$  in the above formulations.

## COMPUTED RESULTS AND REMARKS

Effects of submerged conditions on the dynamic response of soil deposits are examined for a homogeneous soil profile shown in Fig. 1. The present formulation requires dividing the soil into multi-layers for computation. In the first study, however, only one layer is used in order to avoid complexity in the results and to see the essence of coupled behavior of solid skeleton and pore fluid. Fig. 2 shows wave number dispersion curves for various conditions. The imaginary and real parts of  $h$  define respectively the wave length and the rate of decay of Rayleigh waves according to  $e^{-ihx}$ . The mode 1 and 2 denoted in the dispersion curves for dry soil are associated respectively with S-wave and P-wave. When the soil is dry, those mode waves are not progressive at the frequencies below the natural frequencies of the soil deposits associated with S-wave and P-wave respectively for the first and second modes. Above those natural frequencies, they are progressive to form waves in  $x$  direction. When the condition is submerged and undrained, the high pore fluid stiffness increases the P-wave velocity and therefore the mode 2 wave does not propagate until the frequency substantially higher than that for dry soil. When this mode wave is not progressive, the displacements decay somewhat more quickly with distance than those for dry condition . The pore fluid stiffness affects the S-wave velocity very little and therefore the natural frequencies of the soil associated S-waves. When the condition is submerged and drained, one additional mode exists in this case as seen in Figs. 2c and 2d because of the additional degree of the freedom due to the fluid motion. In the case  $k = 10^{-3}$  m/s, the first and second mode waves are very similar

to those observed for undrained condition but the third mode wave is a progressive wave at any frequency and decays very quickly with  $x$ . As is seen in Fig. 3, the fluid motion relative to the solid motion in the third mode is rather independent of permeability although those in other two modes decrease with decreasing permeability. When the relative fluid motions are large, a strong coupling develops between the pore fluid and soil skeleton. As a result, the dispersion curves associated with the mode 1 and 2 are significantly affected by the coupling and thus afore-mentioned difference between the two types modes are not clear as is seen for  $k = 10^{-1}$ m/s case.

A completely flexible massless vertical impermeable wall is assumed to be inserted at  $x = 0$  in the ground and subjected to either a vertical or lateral concentrated harmonic load at the location of the ground surface. Ground displacements are computed along the ground surface by using the above computed wave numbers and mode shapes and are shown in Fig. 4 for  $\omega H/v_s = 2$ . The horizontal and vertical motions are uncoupled with each other for dry soil with  $\nu = .25$  and are governed respectively by the first mode and second mode waves. Therefore, according to the real and imaginary parts of  $h_s$  at  $\omega H/v_s = 2$  in Fig. 2a, the vertical displacements monotonically decay with distance  $x$  because of no real part  $h_s$  in the first mode, whereas horizontal displacements form wave pattern with the wave length defined by the real part of the first mode wave  $h_s$ . When the soil is submerged, the horizontal and vertical motions are coupled each other even with  $\nu = 0.25$  and thus both horizontal and vertical motions form wave pattern in  $x$  as soon as the first mode wave propagates. The difference in the imaginary part of  $h_s$  in the first mode wave between the dry and submerged conditions can be clearly seen in difference in wave lengths along  $x$ . The amplitudes and phase shifts of the displacements of the wall are shown in Fig. 5a at various frequencies for dry soil and submerged soil in undrained condition. The first peaks are due to the first mode wave and are located around the fundamental natural frequency of the soil deposits associated with S-wave ( $\omega H/v_s = \pi/2$ ). The second peaks, clearly seen in  $z$  direction displacements, are due to the second mode

wave and are located around the fundamental natural frequency of the soil deposits associated with P-wave ( $\omega H/v_p = \pi/2$  with  $v_p^2 = (\lambda + 2G + \alpha 2Q)/\rho$ ). The difference in pore fluid rigidity affects not only the amplitudes of the response but the location of the second peak. It very little affects the location of the first peak because of its association with S-wave. The relative fluid motions generates damping and therefore suppress the peak as seen in Fig. 5b. As frequency increases, however, the relative fluid motions becomes smaller and the difference between the undrained and drained conditions diminishes. Contrary to this, when the motion becomes slow, there is enough time for pore fluid diffusion and thus the submerged soil behavior is closer to that of the dry soil as frequency decreases.

Now the soil responses to the wall motions are recomputed by dividing the soil into 10 layers (see Fig. 1), in order to see the distributions of responses along the depth. The computed amplitudes of displacements and pressures at the wall are shown respectively in Figs. 6 and 7 at  $\omega H/v_s = 2$  for various permeabilities of the soil. It is noted that the displacement responses for  $k = 10^{-1}$  m/s and  $10^{-5}$  m/s are very little different respectively from those for dry case and undrained case at the frequency considered. The lower the permeability is, the higher the pore fluid pressure is induced due to more difficulty in pore fluid diffusion. In addition, free drainage at the ground surface affects the distribution of pore fluid pressure giving further complexity in the porewater pressure in the soil. The pore fluid is far stiffer compared with the soil skeleton stiffness and thus the soil responses along the depth are affected by the difference in permeability as seen in those figures.

Three different conditions are considered as shown in Fig. 8 for an identical nonhomogeneous soil profile shown in Fig. 1: they include dry soil (case A), submerged soil with water level at the ground surface (case B) and submerged soil with water level above the ground surface (case C). The shear wave velocities of the inhomogeneous soil are defined so that its fundamental natural frequency is identical to that of the

homogeneous soil. Similar to the previous study, a completely flexible massless vertical wall is assumed to be inserted in the soil and is subjected to a lateral harmonic motion at the surface of the soil. Both of the soil and the water above the soil is divided into 5 layers each for the computation. The computed displacement amplitudes of the wall are shown in Fig. 9 at the ground surface. Clear peaks can be observed around the fundamental natural frequency of the soil associated with S-wave in all three cases. It is interesting to notice that one additional peak exists below this frequency when the water exists above the soil. Again the submerged condition reduces the response significantly. The water body above the soil affects the soil response significantly.

## CONCLUSIONS

A semi-analytical method is developed for dynamic response analysis of fluid-saturated porous medium. The method uses the finite element discretization only along depth and analytical form in lateral direction. The method is found to be numerically very efficient particularly for two-phase mixture problems. The pore fluid in the soil mass affects the dynamic response of the soil deposits by not simply increasing the stiffness of the soil but also by coupling the soil skeleton motions with pore fluid motions. All those effects are affected by the loading rate relative to the pore fluid diffusion rate, boundary conditions and stress gradient. The coupling effects are more predominant for higher permeability soils. When the permeability is low, a mode wave transmitted primarily to the fluid is distinctly different from those primarily transmitted to the soil skeleton and decays very quickly with distance. Under the static and drained conditions, the submerged soil response is identical to the dry soil. Under the dynamic condition, however, the transient pore fluid redistribution depends on the rate of loading and permeability of the soil. The response of submerged soil is closer to the undrained conditions when the combination of those are less favorable for pore fluid movement. The larger the pore fluid motions relative to the soil skeleton are, the higher the damping

generated. When the soil is submerged below the water table, the water above the soil deposits can affect the dynamic response of the soil significantly and thus has to be taken into account in the dynamic response analysis of submerged soil under the water.

## ACKNOWLEDGEMENTS

This work is sponsored by the Minerals Management Service, the U. S. Department of Interior. Mr. Charles Smith of the Minerals Management Service managed the project. The authors express their appreciation to the Port and Harbor Research Institute, the Japan Ministry of Transport for allowing the second author to participate in this research at the University of California at San Diego.

## APPENDIX I REFERENCES

- Biot, M. A., 1956, "Theory of Wave Propagation of Elastic Waves in a Fluid-Saturated Porous Solid, Part I: Low Frequency Range and Part II High Frequency Ranga," J. Accoust. Soc. America, Vol. 28, pp. 168-191.
- Dresiewicz, H., 1970, "The effect of boundaries on Wave Propagation in a Liquid-filled Porous Solid," Bull. Seism. Soc. America, Vol 15, pp. 599-607.
- Foda, M. and Mei, C. C., 1982, "Boundary Layer Theory for Rayleigh Waves in a Porous, Fluid-Filled Half Space," Proc. Soil Dynamics and Earthquake Engineering Conference, Southampton, July, pp. 239-249.
- Ghaboussi, J. and Wilson, E. L., 1978, "Variational Formulation of Dynamics of Fluid-Saturated Porous Elastic Solids," J. Eng. Mech. Div., ASCE, EM4, pp.947-963.
- Jones, J. P., 1961, "Rayleigh Waves in a Porous Elastic Fluid Saturated Solid," J. Accoust. Soc. America, Vol. 33, pp. 969-962.
- Kausel, E. and Roesset, J. M., 1975, "Dynamic Stiffness of Circular Foundations," J. Eng. Mech. Div., ASCE, Vol. 101, EM6, pp. 771-785.
- Lysmer, J. and Waas, G., 1972, "Shear Waves in Plane Infinite Structures," J. Eng. Mech. Div., ASCE, Vol. 98, EM1, pp. 85-105.
- Prevost, J. H., 1982, "Nonlinear Transient Phenomena in Saturated Porous Media," Comp. Mech. Appl. Mech. Eng. Vol. 20, pp. 3-8.

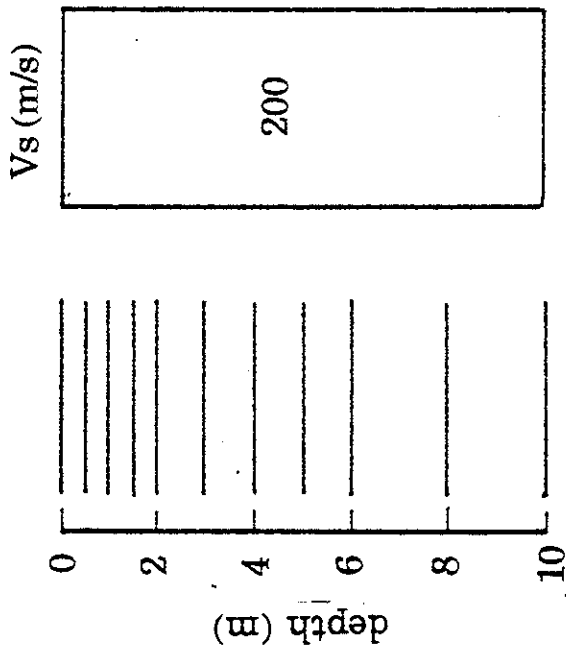
Simon, B. R., Zienkiewicz, O. C. and Paul, D. K., 1986, "Evaluation of  $u-w$  and  $u-\pi$  Finite Element Methods for the Dynamic Response of Saturated Porous Media Using One-Dimensional Models," *Int. Numer. Anal. Methods Geomech.*, Vol. 10, pp. 461-482.

Simon, B.R., Zienkiewicz, O. C. and Paul, D. K., 1984, "An Analytical Solution for the Transient Response of Saturated Porous Elastic Solids," *Int. Numer. Anal. Methods Geomech.*, Vol. 8, pp. 381-398.

Tajimi, H. and Shimomura, Y., 1976, "Dynamic Analysis of Soil-Structure Interaction by the Then Layered Element Method," *Transactions of the Architectural Institute of Japan*, Vol.243, pp.41-51 (in Japanese).

Zienkiewics, O. C. and Shiomi, T., 1984, "Dynamic Behavior of Saturated Porous Media: Generalized Biot Formulation and Numerical Solution," *Int. J. Numer. Anal. Methods Geomech.*, Vol. 8, pp. 71-96.

(a) Homogeneous profile

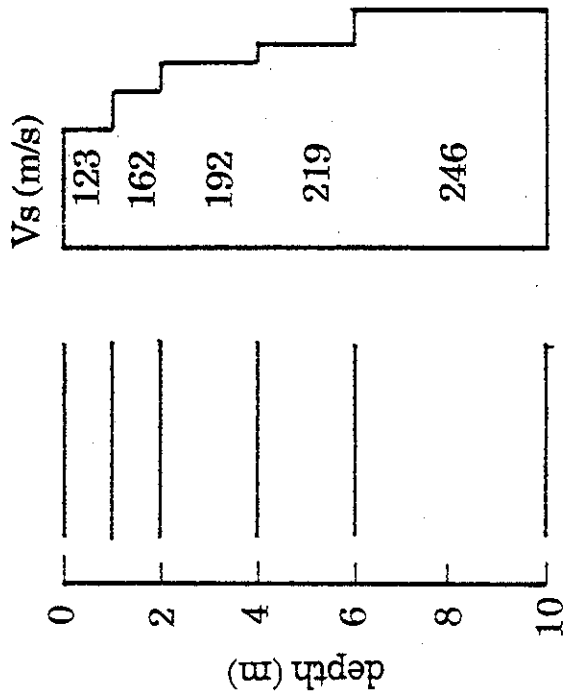


$$K_s = 3.7 \times 10^6 \text{ tf/m}^2$$

$$v = 0.25$$

$$n = 0.375$$

(b) Inhomogeneous Profile

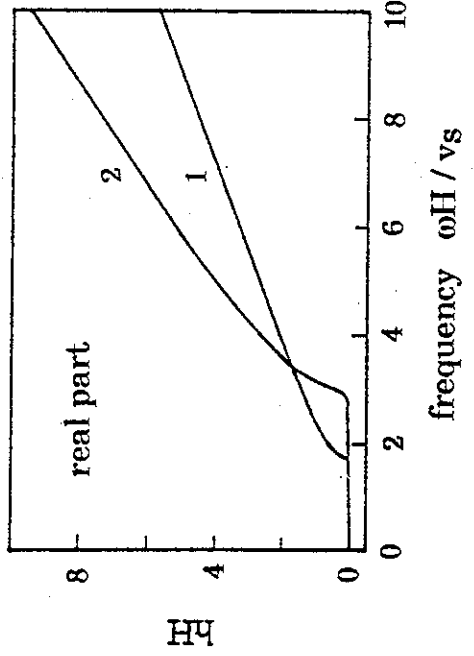
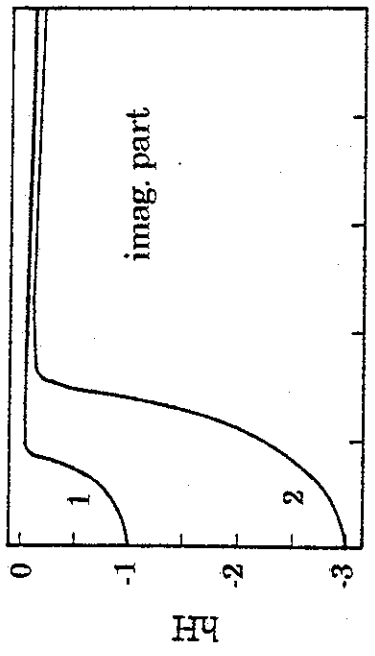


$$K_f = 2.08 \times 10^5 \text{ tf/m}^2$$

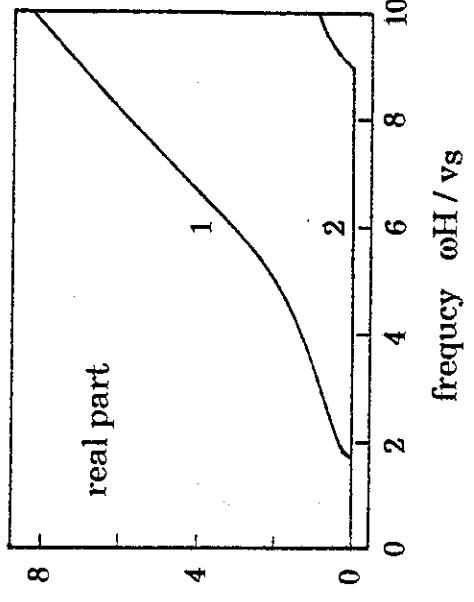
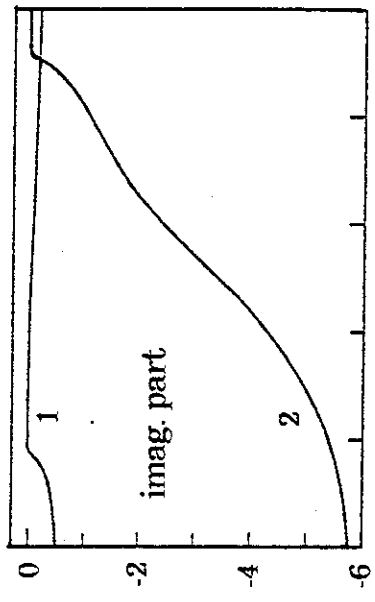
$$D = 2 \%$$

$$\gamma = 2.6 \text{ tf/m}^3$$

Fig. 1 Homogeneous and inhomogeneous soil profiles

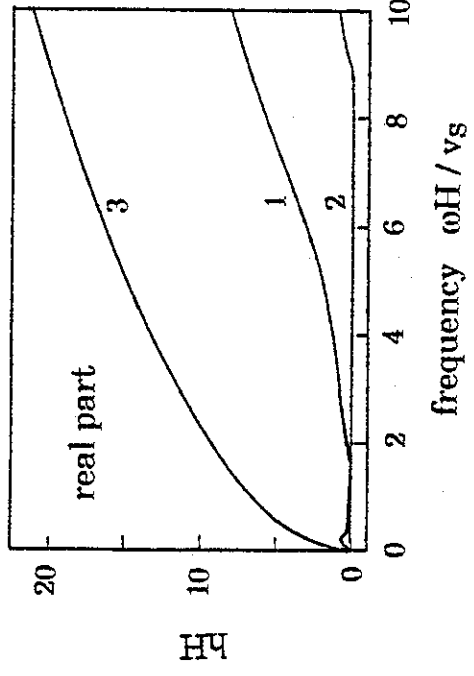
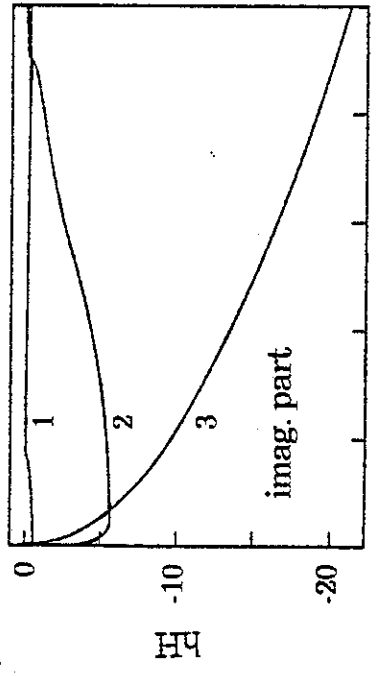


(a) Dry soil

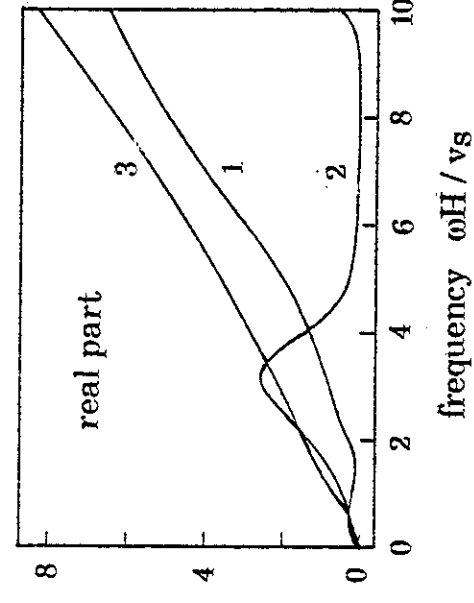
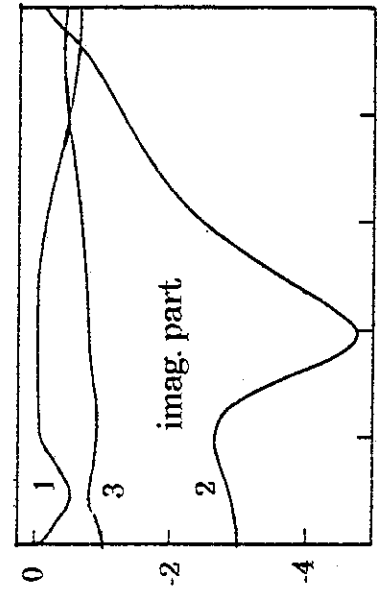


(b) Submerged soil in undrained condition

Fig. 2a, 2b Wave number dispersion curves



(c) Submerged soil in drained condition ( $k = 10^{-3}$  m/s)



(d) Submerged soil in drained condition ( $k = 10^{-1}$  m/s)

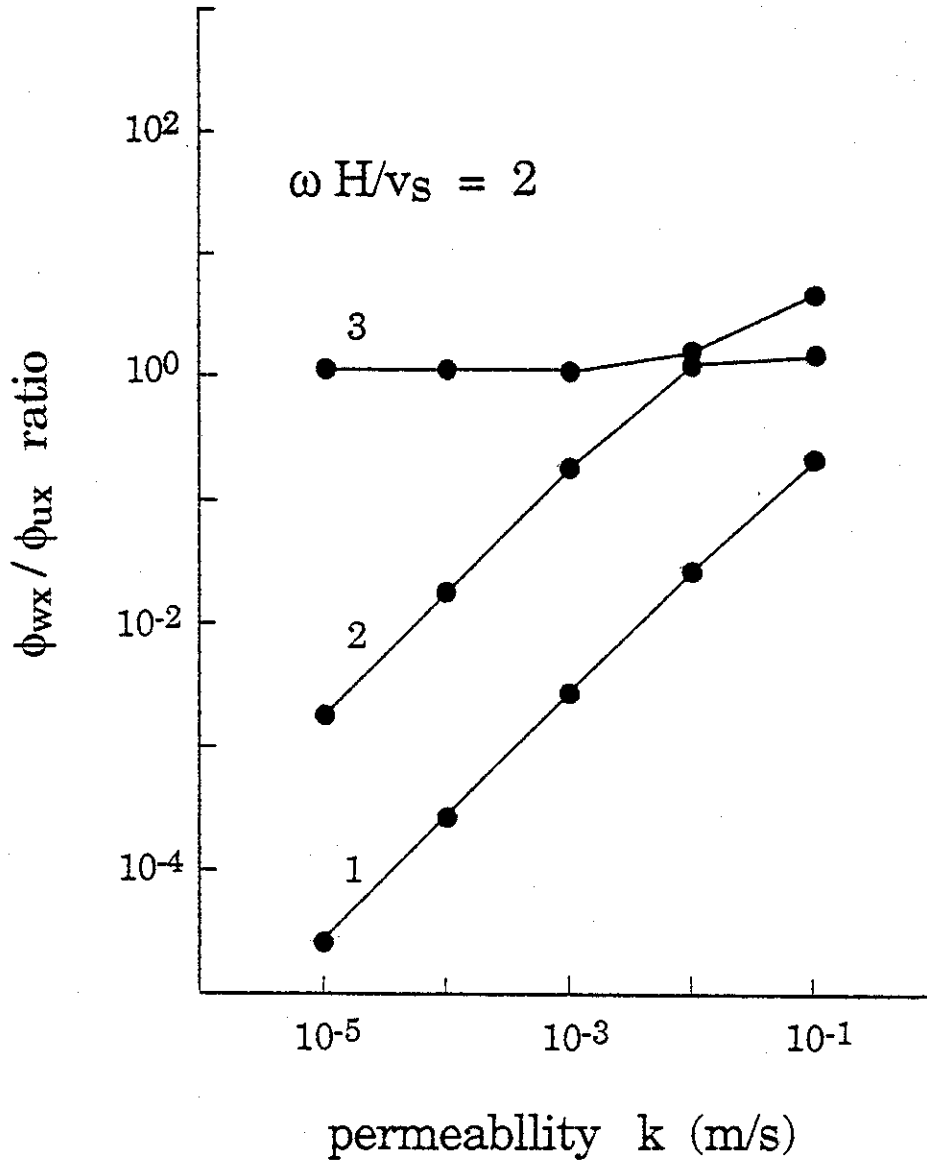
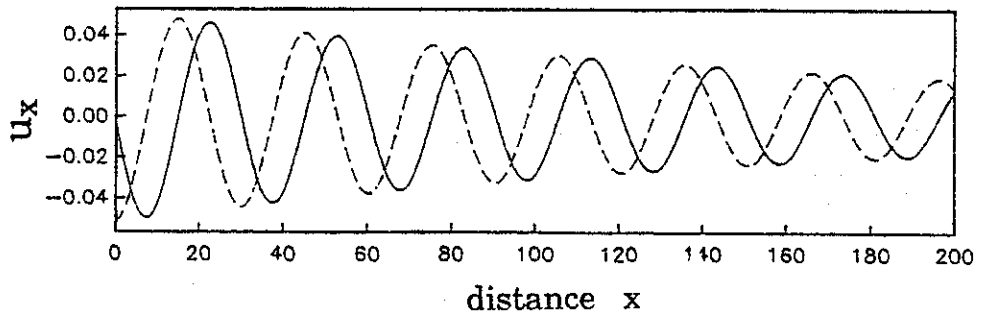
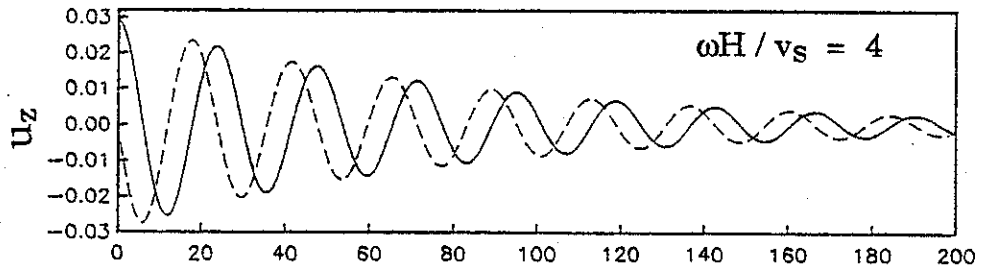
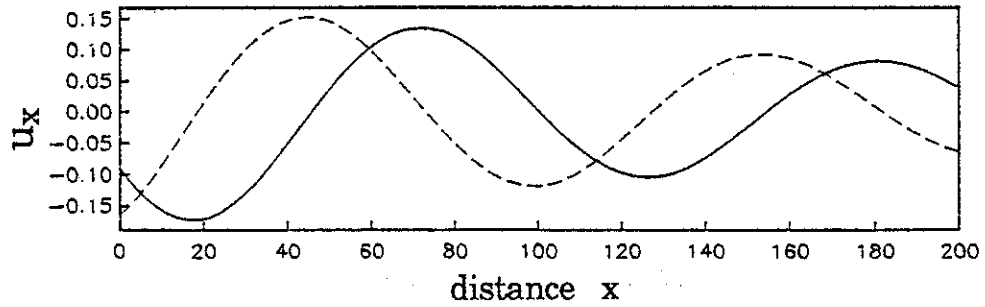
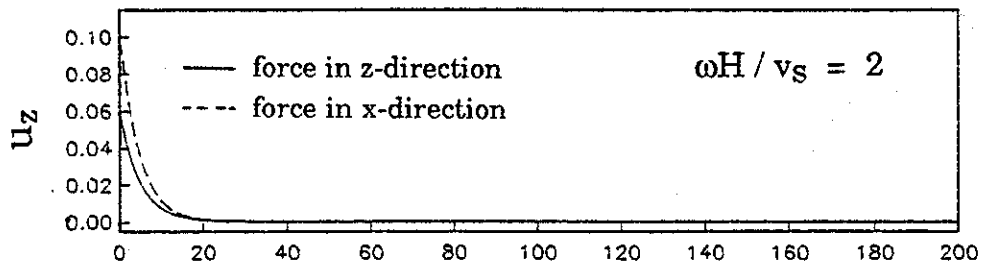
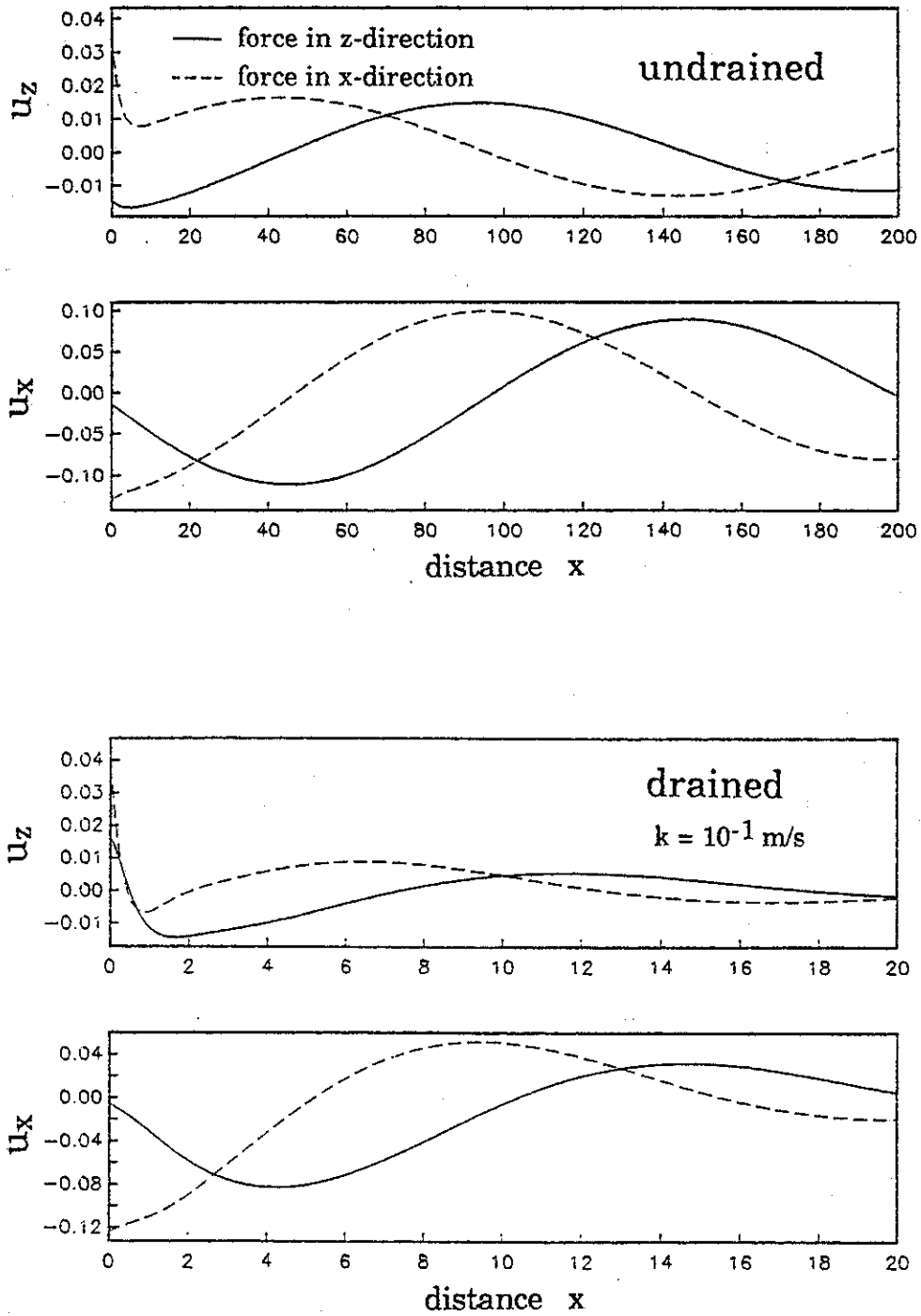


Fig. 3 Variation of  $\phi_{wx} / \phi_{ux}$  ratio with permeability



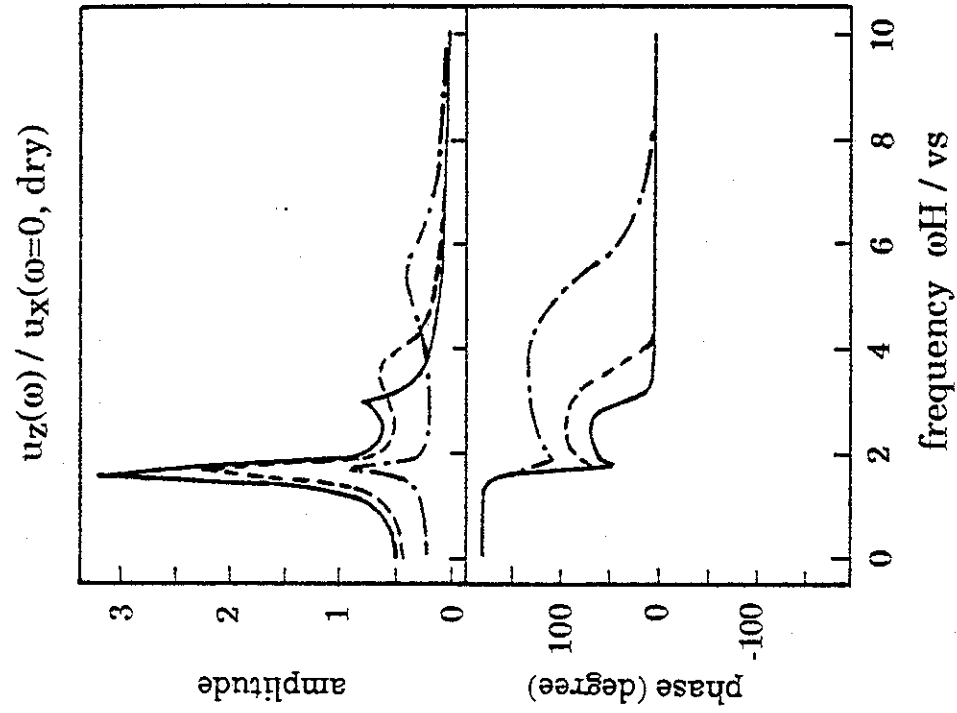
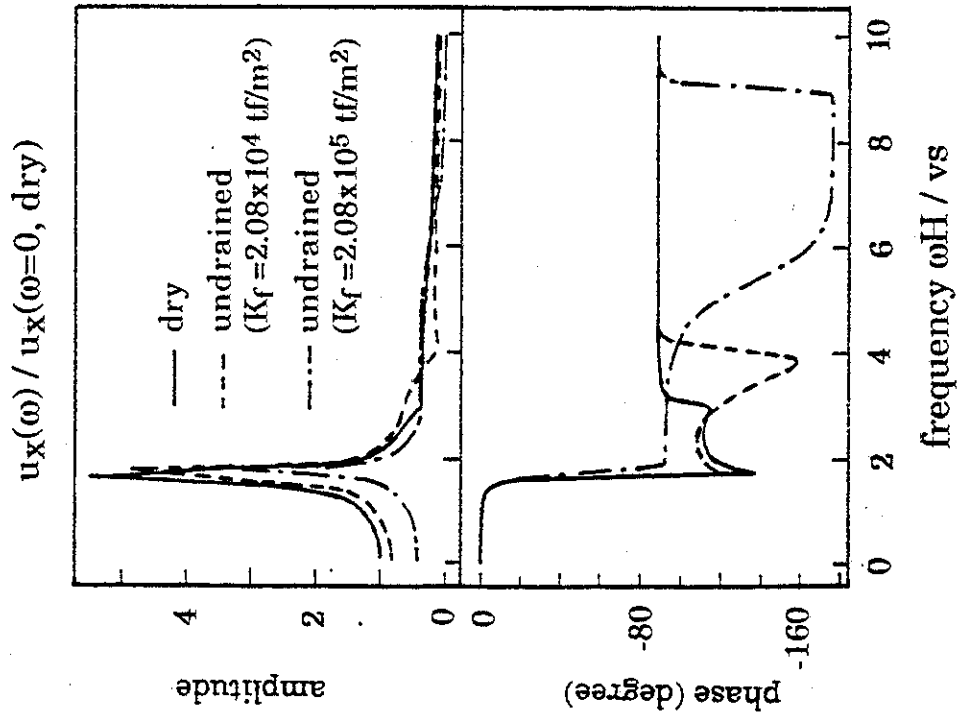
(a) Dry soil ( $\omega H / v_s = 2$  and  $\omega H / v_s = 4$ )

Fig. 4a Displacement amplitudes at various  $x$  along the ground surface



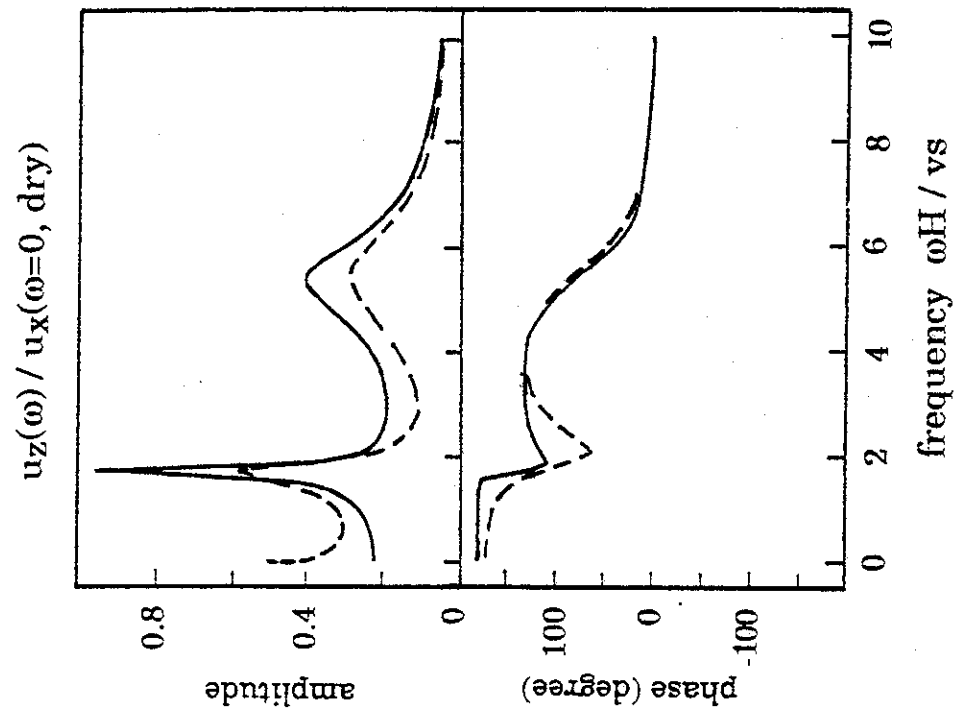
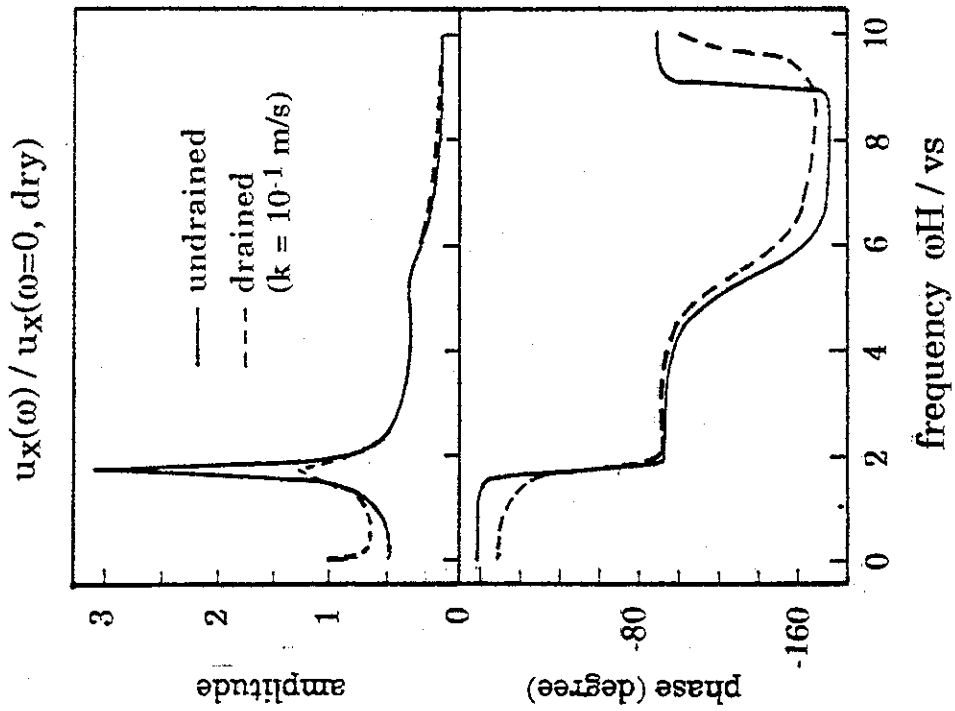
(b) Submerged soil in undrained and drained condition  
 $(\omega H / v_s = 2)$

Fig. 4b Displacement amplitudes at various  $x$  along the ground surface



(a) dry soil and submerged soil in undrained condition

Fig. 5a Displacements at the top of the vertical wall subjected to lateral vibration



(b) submerged soil in undrained and drained condition

Fig. 5b Displacements at the top of the vertical wall subjected to lateral vibration

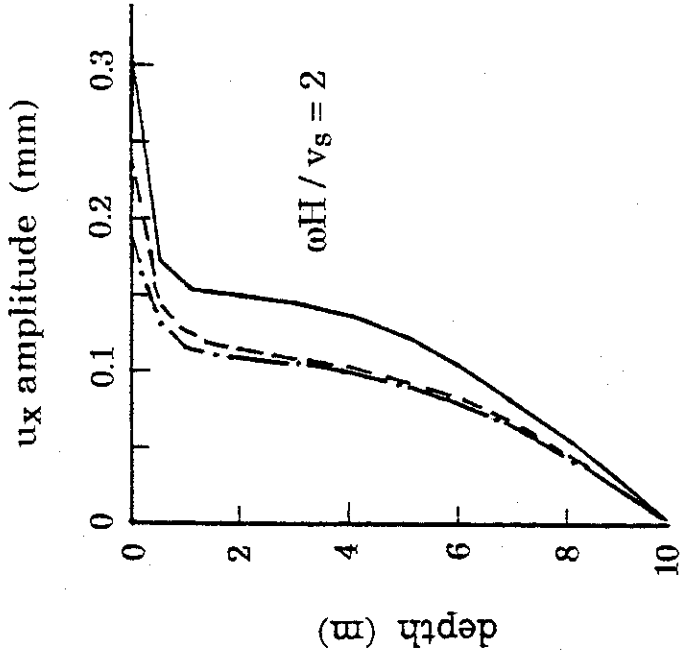
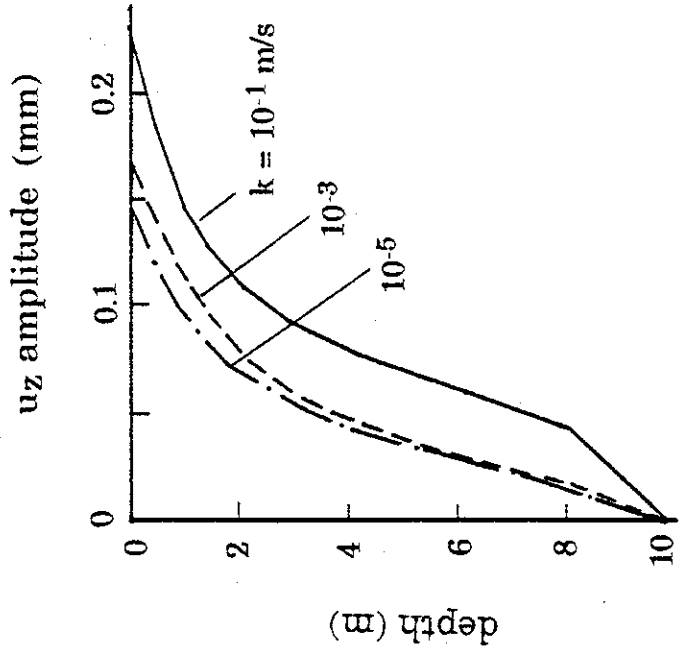


Fig. 6 Displacement response amplitudes of the wall along depth

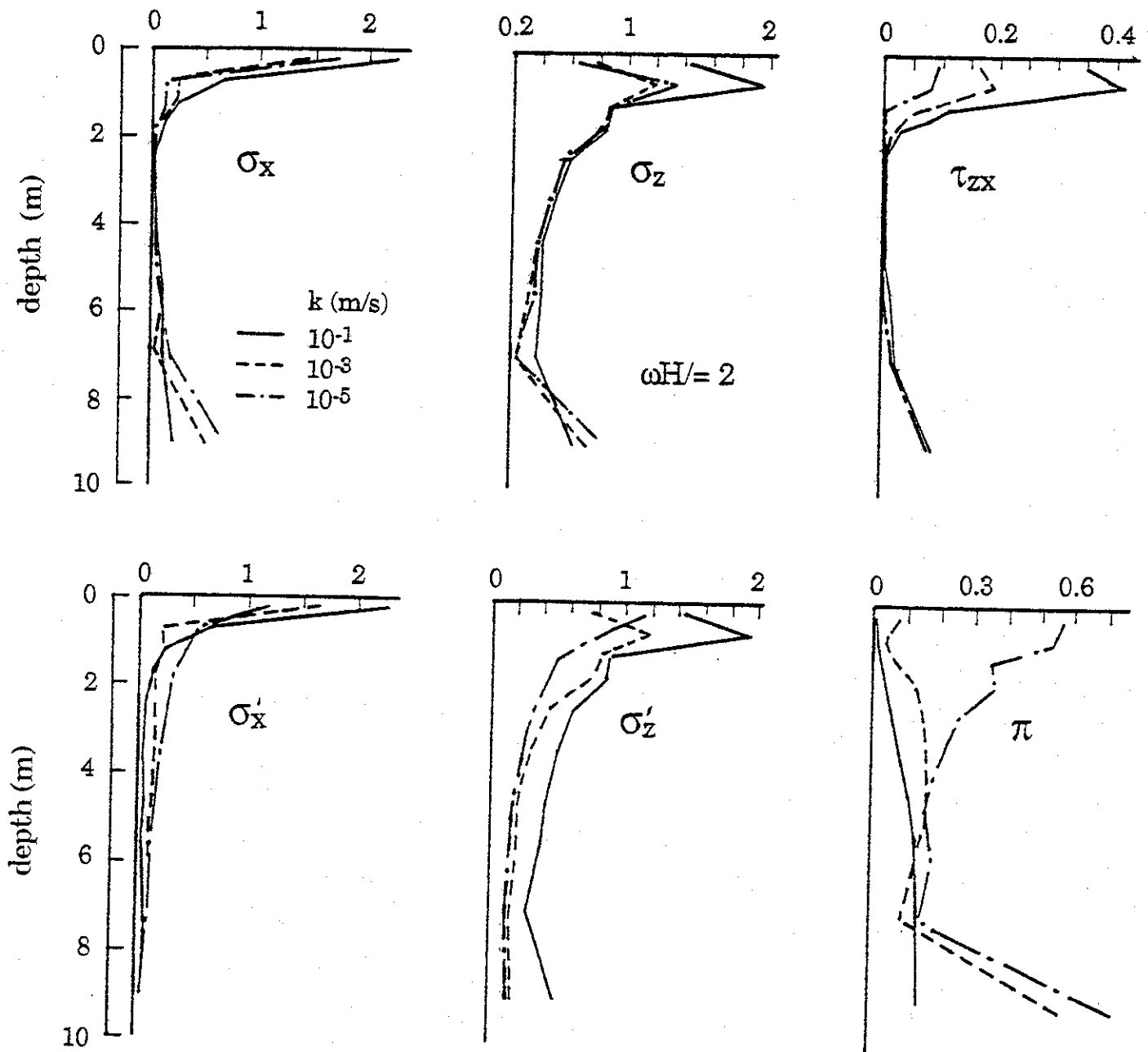


Fig. 7 Pressure response amplitudes at soil-wall interface along the wall

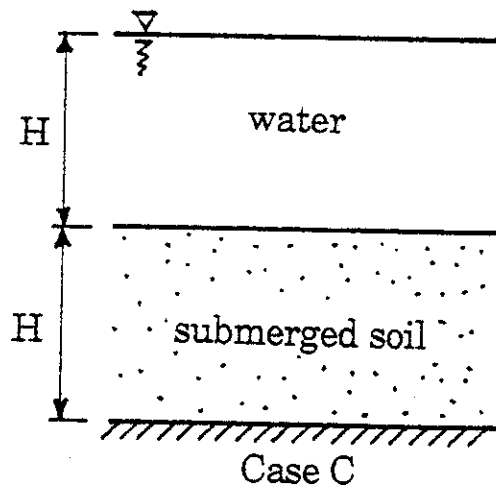
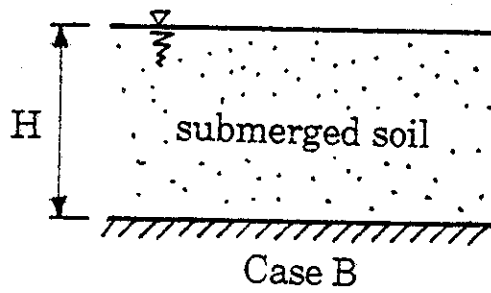
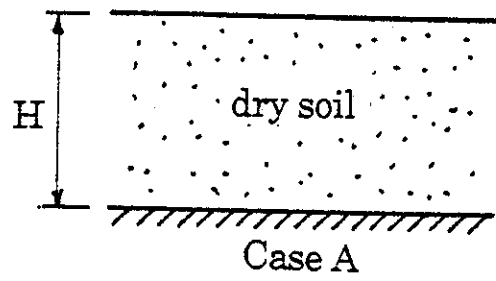


Fig. 8 Various cases considered for examples

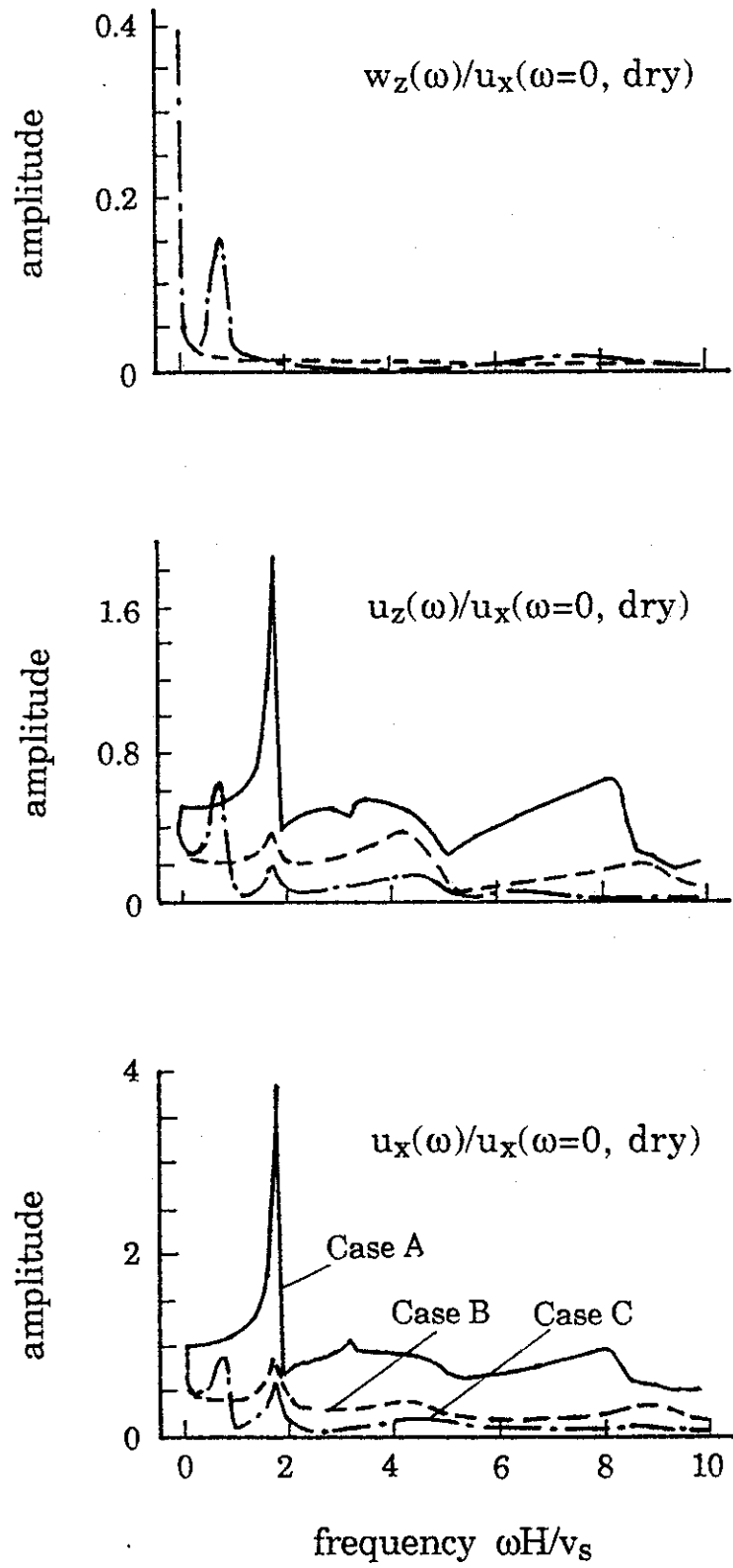


Fig. 9 Lateral displacement amplitudes at the top of the wall subjected to lateral vibration